J Fluoresc (2011) 21:1239–1247
DOI 10.1007/s10895-010-0803-1

ORIGINAL PAPER

Photophysical Properties of Rare Earth (Eu^{3+}, Sm^{3+}, Tb^{3+}) Complex Covalently Immobilized in Hybrid Si-O-B Xerogels

Chang Wang · Bing Yan

Received: 13 October 2010 / Accepted: 28 December 2010 / Published online: 14 January 2011

Abstract The molecular linkage (phenSi) from functionalized 5-amino-1,10-phenanthroline ($PhenNH_2$) by 3-(triethoxysilyl)-propyl isocyanate (TESPIC) is to construct the rare earth (Sm^{3+}, Eu^{3+}, Tb^{3+}) center covalently immobilized in the hybrid xerogels of Si-O-B through the cohydrolysis and copolycondensation process between different alkoxide precursors of them (tetraethoxysilane (TEOS), tri-n-butylborate (TBB)). NMR, FTIR and ultraviolet absorption are measured to confirm the obtained materials. X-ray diffraction patterns revealed the hybrid materials are amorphous. Scanning electronic microscopy images show the stripe microstructure without phase separation phenomenon in the obtained hybrid materials. The covalently bonded Si-O-B hybrid xerogel presents the similar photoluminescent behavior to the pure Si-O-Si hybrid xerogels, which indicates that Si-O-B hybrid xerogel is a suitable system for the luminescence of RE^{3+}.

Keywords Rare earth ion · Si-O-B hybrid xerogel · Photophysical property · Luminescence

Introduction

It has long been recognized that trivalent rare earth ions have excellent luminescent properties in the visible and near-infrared region, for example large stokes shift, high luminescence quantum efficiency, and narrow line emission spectrum *etc.*, for which they are applied in all kinds of practical fields such as phosphors, devices and biological images [1–3]. However, rare earth ions themselves have not been widely and directly applied to luminescent materials for a long period, which is mainly due to their low molar absorption coefficients aroused by spin-forbidden f-f transitions so that the direct photoexcitation of rare earth ions is not efficient. So the possibility to improve the luminescence of rare earth ions can be achieved through two basic paths. One is to dope the photoactive RE^{3+} into the special matrices such as all kinds oxides and oxysalts, which has been extensively investigated for the phosphors [4, 5]. Another path is to design rare earth complexes comprising sensitizing ligands such as β-diketones, aromatic carboxylic acids and heterocyclic ligands duo to their excellence coordination ability and proper energy level match. But these molecular systems still possess poor stability for practical applications [6, 7]. To overcome the disadvantages, rare earth complexes can also be fabricated into inorganic matrices as photoactive species to integrate the photophysical properties of the organic component and the favorable thermal and mechanical characters of the inorganic networks simultaneously [8, 9].

While the above mentioned hybrids of doping rare earth complexes into the inorganic matrix often encounter some problems such as the quenching effect of luminescent centers, inhomogeneous dispersion of two phases and leaching of the photoactive molecules with a low concentration of the complex because only weak interactions exist between the organic and inorganic phases [10, 11]. So the stratum to solve the problem is to chemically link the rare earth complex species to the inorganic matrix through unique functional molecular bridge [12–24]. To presence, all kinds of typical ligands of rare earth ions have been functionalized as molecular bridge to assemble the hybrids [12–24]. On the basis of these work, some rare earth

C. Wang · B. Yan (✉)
Department of Chemistry, Tongji University,
Siping Road 1239,
Shanghai 200092, People's Republic of China
e-mail: byan@tongji.edu.cn

hybrids with organically modified mesoporous hybrids can be achieved [24, 25]. Furtherly, the polymers can be introduced to obtain multicomponent polymeric hybrids [26, 27]. In nature, these hybrids embody the features of both rare earth doped phosphors an rare earth complexes because the organically functionalized Si-O component can behave two roles of host and ligand. So the luminescence of them can be enhanced remarkably.

Most of these hybrids are prepared with sol–gel technology and organically modified silica based materials are mainly focused on for the hydrolysis and polycondensation process of the alkoxysilanes for they are easily controllable [12–27]. But it can be expected to realize the assembly of the hybrid systems with other inorganic network [21, 28] and even the multi-component hybrid host network [29]. Unfortunately, the luminescence of titanate-based hybrid xerogel is weaker than that of silica one [21, 29]. So it is necessary to study the construction of rare earth hybrid material systems with other hybrid xerogels. In this paper, 5-amino-1,10-phenanthroline is used as the functional molecular bridge which can both coordinate to rare earth ions and link the rare earth complexes to inorganic matrix with covalent bonds after being modified by coupling agent (TESPIC). The photoluminescent properties of them are studied in detail.

Experimental Section

Starting Materials Rare earth nitrates are obtained by dissolving their oxides (Sm_2O_3, Eu_2O_3, Tb_4O_7) in concentrated nitric acid. Tetraethoxysilane (TEOS) is distilled and stored under a nitrogen atmosphere. 3-(triethoxysilyl)-propyl isocyanate (TESPIC) are purchased from the Lancaster Company. The key material, 5-amino-1,10-phenanthroline (denoted $phenNH_2$) is prepared according to the literature procedures [30]. Tetraethyl orthosilicate, titanium butoxide and tributyl borate are commercially available and used without purification. The solvents (THF, DMF) used are purified by common methods. The other reagents are analytically pure.

Synthesis of Precursor phenSi The precursor phenSi is prepared according to the previous literature [15, 30]. $phenNH_2$ (0.212 g, 1 mmol) is first dissolved in 20 mL of $CHCl_3$, and 2 mL of TESPIC is then added dropwise to the solution while stirring. The solvent is removed at atmospheric pressure, and the resulting mixture is stirred overnight at 80 °C. After cooling to room temperature, Cold hexane is added to the mixture and a white precipitate is obtained. The white precipitate (phenSi) is filtered off, ished with cold hexane and dried in vacuo. The ^1H NMR ($CDC1_3$, 400 MHz) data of phenSi are as follows: 0.52 (4H, m), 1.13 (18H, t), 1.60 (4H, m), 3.20 (4H, m), 3.68 (12H, q), 7.18 (2H, s), 7.68 (2H, m), 7.86 (1H, s), 8.24 (2H, m), 9.23 (2H, m).

The Synthesis of the Rare Earth Hybrid Xerogel An appropriate amount of phenSi is introduced into N, N-dimethyl formamide (DMF) by stirring in the beaker. And then a stoichiometric amount of $RE(NO_3)_3{\cdot}6H_2O$ is added to the solution. Two hours later corresponding amount of tetraethyl orthosilicate is put into the break then the mixture is stirred for 8 h strongly at room temperature to obtain a single phase and transferred to the 80 °C oven for 5 days aging. Whereafter, the product RE-phenSi-O-Si is taken out and grinded into powder for optical characterization. The mole ratio of $RE(NO_3)_3{\cdot}6H_2O$/phenSi/TEOS/H_2O is 1: 2: 12: 48. Using the same method we have synthesized RE-phenSi-O-B by employing tributyl borate to replace tetraethyl orthosilicate. In addition, for further study properties of these hybrid materials we have prepared ternary complexes grafted onto silica and titanium network TTA-RE-phenSi-O-B. The scheme for the possible composition and predicted structure of binary and ternary hybrids are shown in Fig. 1.

Physical Measurements All measurements are completed under room temperature. 1H NMR spectra are recorded on a Bruker AVANCE-400 spectrometer with tetramethylsilane (TMS) as internal reference. FTIR spectra are recorded on a Nicolet model 5SXC spectrophotometer using the KBr

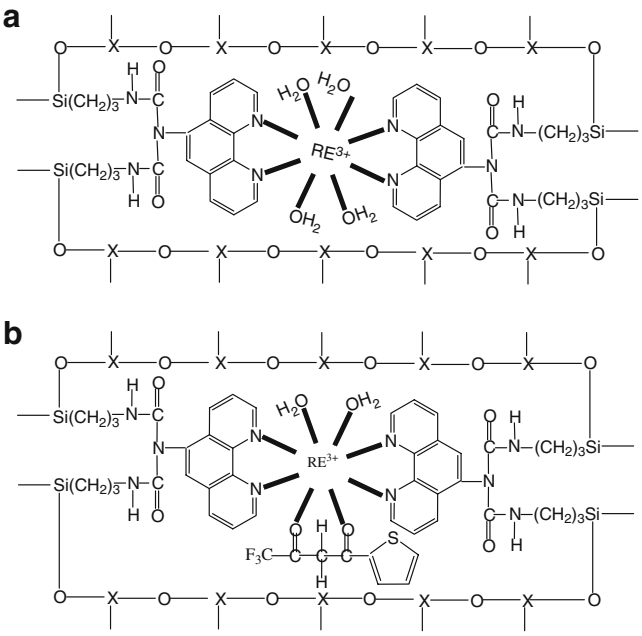

Fig. 1 The scheme of the synthesis process of binary and ternary hybrid xerogels (**a**) RE-phenSi-O-Si(B) and (**b**) TTA-RE-phenSi-O-Si(B)

pellet technique. Ultraviolet absorption spectra are recorded on an Agilent 8453 spectrophotometer. The microstructure is estimated by a scanning electronic microscope (Philips XL-30). Ultraviolet–visible diffuse reflection absorption spectra are obtained on a BWS003 spectrophotometer. X-ray powder diffraction patterns are recorded on a BRUKER D8 diffractometer (40 mA/40 kV) using monochromated CuKα1 radiation (λ=1.54 Å) over the 2θ range of 10° to 70°. Fluorescence excitation and emission spectra are recorded on a RF-5301 spectrofluorophotometer. Luminescent lifetimes are obtained with an Edinburgh FLS 920 phosphorimeter using a microsecond pulse lamp as excitation source.

Results and Discussion

Figure 1 shows the scheme for the predicted composition and structure of the binary hybrid xerogels RE-phenSi-O-Si (B) and ternary hybrid xerogels TTA-RE-phenSi-O-Si(B). These hybrid xerogels are all noncrystalline state and so it is almost impossible to confirm the exact structure of them and the coordination behavior of the rare earth ions. However, according to the rare earth coordination chemistry principle and the functional group of organic unit of the linkage, the main composition about these hybrid materials can be predicted. As we known, the phenSi possesses the coordination ability of the two nitrogen atoms of phen groups and TTA ligand provides the two chelated oxygen atoms of its two carbonyl groups. The remaining coordination position can be occupied by the H_2O molecules. Considering the most common coordination number of RE^{3+} is eight, the scheme fot the binary and ternary hybrid xerogels can be shown in Fig. 1(a), (b). This can be further proved by the FT-IR spectra and photoluminescence.

The FTIR spectra of the free ligand phenNH_2 and linkage phenSi are measured. The absorption bands to the vibration of NH_2 group of phenNH_2 at about 3300–3400 cm^{-1} range disappear in the FT-IR spectra of phenSi, while some absorption bands at around 2900–3000 cm^{-1} appear, corresponding to the vibrations of the methylene (-CH_2-) groups of TESPIC. The stretching vibration located at 2285–2385 cm^{-1} for N=C=O of TESPIC can not be observed. Besides, the stretching vibration of Si–C located at 1165 cm^{-1}, the stretching vibration of Si–O at 1110 cm^{-1} and 1072 cm^{-1}, and C=O feature absorption band of 1702 cm^{-1} can be found, suggesting that TESPIC has been grafted onto the NH_2 group of phenNH_2. The completion of the grafting reaction between phenNH_2 and TESPIC can be also confirmed by the ultraviolet absorption spectra. Comparing the ultraviolet absorption spectra (DMF as solvent) of phenNH_2 and phenSi, an obvious blue shift of the major π-π* electronic transitions (from 280 nm to 276 nm and from 341 nm to 323 nm) can be observed, indicating that the electron distribution of phenSi has changed compared to phenNH_2 duo to the introduction of TESPIC. So, we predict that the ligand phenNH_2 has been successfully modified by TESPIC. These results take agreement with the reports in ref. [15]

In order to study the properties of lanthanide hybrid xerogels, we also prepare the hybrids of pure silica hybrid xerogels for comparison. Figure 2 shows the selected FTIR spectra of binary and ternary europium hybrids of hybrid xerogels. The high frequencies ranges in 3400~3600 cm^{-1} can be ascribed to the stretching vibration of O-H group [31]. The absorption peaks within the 1050~1355 cm^{-1} are originated from the stretching vibrations of Si-O-Si and Si-O-B bonds, respectively [32]. Unfortunately, it is not shown the distinction between Si-O-B and Si-O-B clearly. Furthermore, the peaks at around 1650 and 1560 cm^{-1} are originated from -CONH- group of the modified organic ligands [15]. The broad absorption of the (ν(Si-O-Si)) vibration located in 1125–1050 cm^{-1} wavelength ranges can be seen in all of the spectra, which indicates the formation of Si-O-Si network during the hydrolysis/condensation reactions. Furtherly, the accomplishment of the coordination reaction of RE^{3+} can be clearly shown by infrared spectroscopy. Meanwhile, the twisting bending vibrations at 855 cm^{-1} which belong to the absorption of hydrogen atoms of phen group have almost disappeared, this fact firmly prove that the phen group can effectively coordinate to the rare earth ions [33]. Besides, the characteristic band of NO_3^- can also be checked at around 1380 cm^{-1}. The formation of H_2O molecule during the

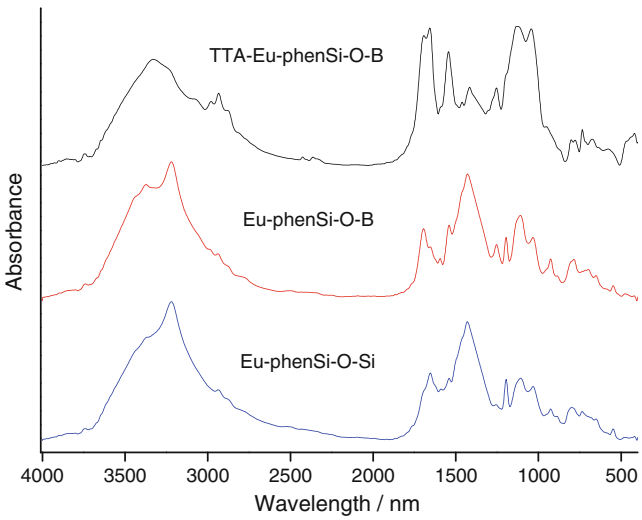

Fig. 2 Selected FTIR spectra of the europium hybrid gels

hydrolysis/condensation reactions can also be clearly indicated by the IR spectra. The vibration signal around 3300 cm^{-1} is the characteristic of H_2O molecule, and the most intense in the spectrum. No apparent distinction can be observed among the different hybrid Si-O-B framework, suggesting the homogeneous sol–gel process to form the uniform hybrid system.

The selected X-ray diffraction patterns of these hybrid materials are shown in Fig. 3, which reveals that all of the hybrid materials with $10° \leq n \leq 70°$ are mostly amorphous. As we known, when a material contains a large crystalline region, the peak observed is usually sharp and its intensity is strong, whereas that of amorphous material is rather broad [34]. All the diffraction curves show the similar broad peaks, with angel 2θ centered around 22°, which are characteristic of amorphous silica materials [35]. It seems that the introduction of TTA has no influence on the disorder structure of the siliceous skeleton. The structural unit distance, is approximately 3.98 Å calculated from Bragg law. This may be ascribed to the coherent diffraction of the siliceous backbone of the hybrid gel [36]. In addition, none of the hybrid materials contains measurable amounts of phases corresponding to the pure organic compound (phenSi or TTA) or free RE nitrate, which is an initial indication for the formation of the true covalent-bonded molecular hybrid materials.

The selected thermogravimetric weight loss curves of pure binary complex Sm-phen, the binary hybrid xerogel materials (Sm-phenSi-O-Si, Sm-phenSi-O-B) are given in Fig. 4. Comparing the three curves, it can be observed that both of the hybrid xerogels shows the higher thermal stability than that of pure complex, indicating that the introduction of the host is favorable for samarium active species. Furtherly, it can be observed that the hybrid

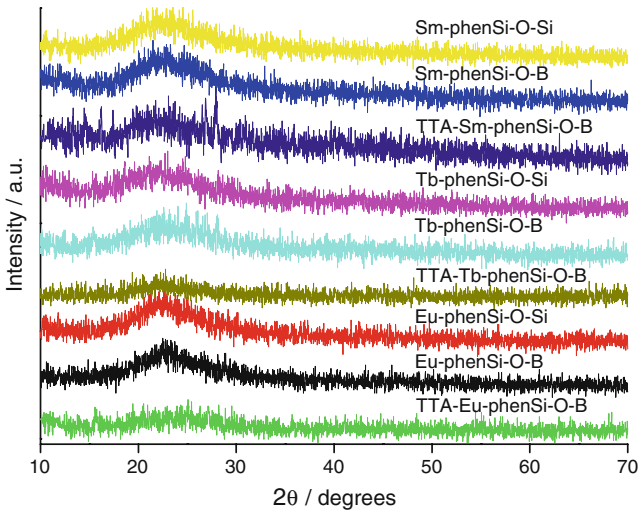

Fig. 3 The selected XRD patterns of rare earth hybrid gels

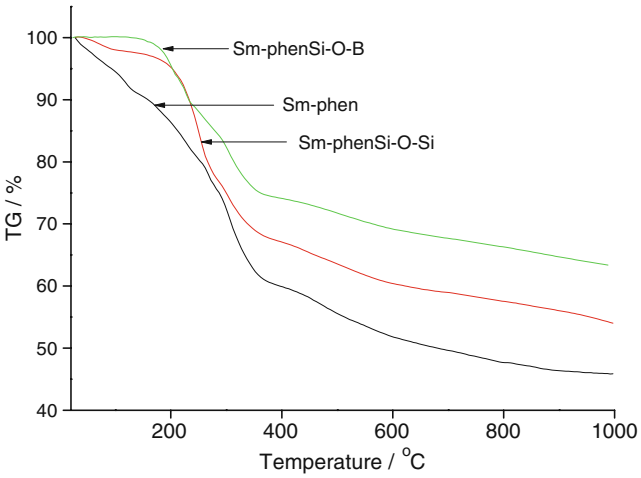

Fig. 4 The selected TG-DSC curves of samarium hybrid gels

materials of hybrid host Si-O-B show the slight weaker thermal stability than pure Si-O-Si host. Both the water loss temperature and the decomposition temperature of organic groups for the hybrid gel with hybrid host show decrease. Subsequently, the pure silica material possesses the higher thermal stability than hybrid Si-O-B materials for the former is more easily to form the homogeneous and uniform system. Furthermore, the hybrid gel of composite host Si-O-B show the lower weight loss than pure hybrid of Si-O-Si, which reveals the hydrolysis and condensation content are higher between hetero-alkoxyl compounds than single alkoxyl silane.

The scanning electron micrographs of the hybrid materials are shown in Fig. 5 (A for Eu-phenSi-O-Si, B for Sm-phenSi-O-Si, C for Eu-phenSi-O-B, D for Eu-phenSi-O-B, E for TTA-Eu-phenSi-O-B, F for TTA-Sm-phenSi-O-B). The uniform frameworks on the surface of all the hybrid materials demonstrate that homogeneous systems containing covalent bonds between the organic precursor (phenSi) and inorganic matrices are obtained. In comparison to hybrid materials with doped rare earth complexes generally experiencing phase separation phenomena, no phase separation can be observed in these hybrid materials and the inorganic and organic phases in the hybrid materials can exhibit their distinct properties together [37]. All these binary or ternary hybrid xerogels materials show the similar stripes microstructure, which is dispersed regularly on the surface of the hybrid material. In addition, some small branches emerge at the end of each side of stripe, and the stripes will continue to grow according to the direction of these branches to form the final structure. This is due to the influence of phenSi in the sol–gel process between phenSi and TEOS (or TBB). The hybrid xerogel materials could be achieved through a copolycondensation reaction between the terminal silanol groups of phenSi and TEOS (TEOS and TBB). At the

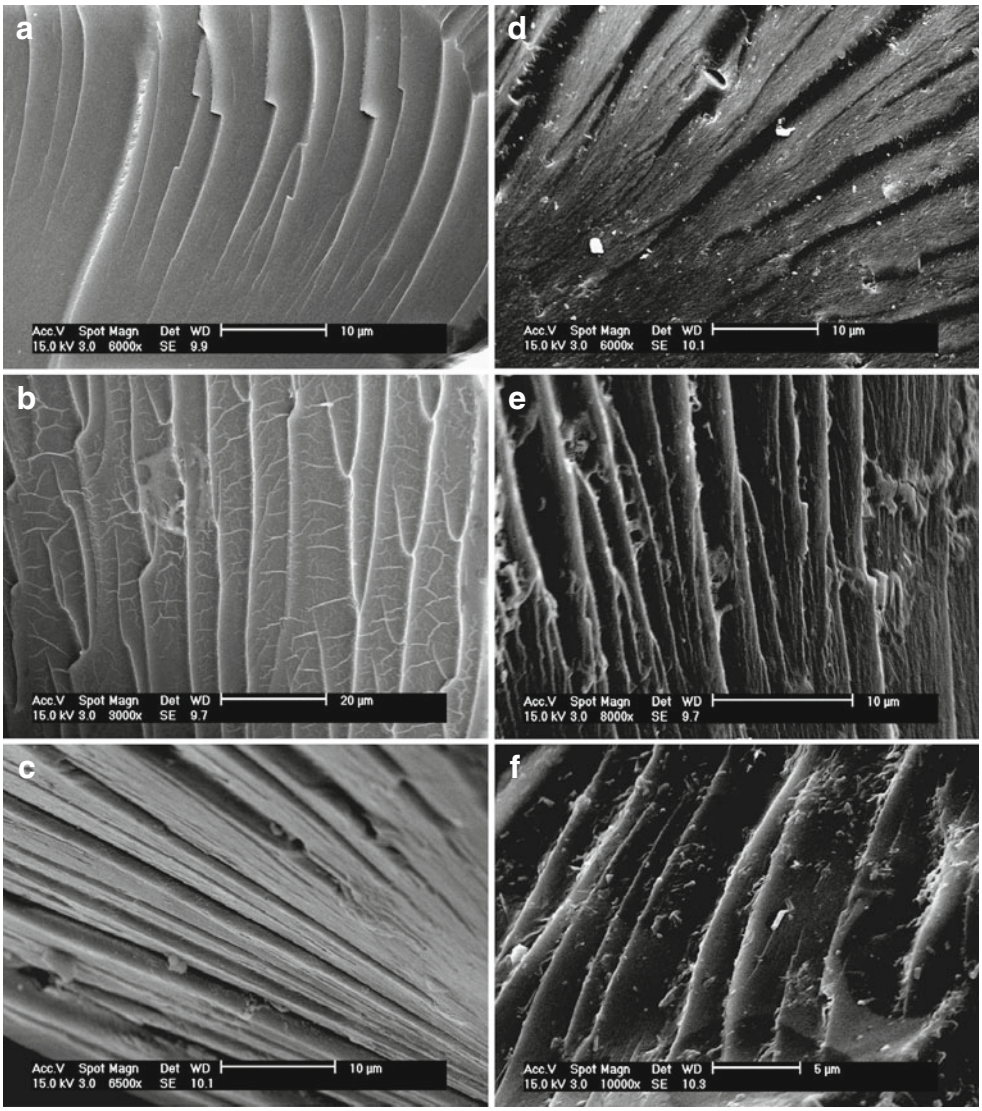

Fig. 5 The selected SEM images of europium and terbium hybrid xerogels: **a** Eu-phenSi-O-Si, **b** Sm-phenSi-O-Si; **c** Eu-phenSi-O-B, **d** Eu-phenSi-O-B, **e** TTA-Eu-phenSi-O-B, **f** TTA-Sm-phenSi-O-B

beginning of the reaction, the individual hydrolysis of phenSi and TEOS (TEOS and TBB) are predominant. Furtherly, it is related to the copolycondensation reactions between hydroxyl groups of both RE-phenSi and TEOS (TEOS and TBB). These chemically bonded hybrid xerogels bearing the RE-O coordination bond and Si-O-Si (B) covalent bonds can also been obtained after the introduction of RE^{3+}. Here we name the cooperation of both RE-phenSi and TEOS (TEOS and TBB) within the in-situ sol–gel process as cohydrolysis and copolycondensation (similar to copolymerization of organic monomer). Furtherly, different rare earth ions, alkoxyl compound precursors (TEOS, TBB) and the second chelated ligand TTA also have some little influence on the microstructure of the final hybrids. The coordination reaction between RE^{3+} and phenSi exists in the in-situ copolycondensation process, which has influence on the sol–gel process and the microstructure or physical properties of the hybrids. The ternary hybrid xerogels shows more complicated stripe microstructure, which maybe the introduction of TTA affects the process of copolycondensation.

UV-visible diffuse reflection spectra are performed on the hybrid materials. Figure 6 shows the selected spectra of Sm^{3+} hybrid xerogels. It exhibits a broad absorption band in the 200–500 nm, which belongs to the whole near-UV range. This absorption band corresponds to transition from the ground state of the organically modified Si-O-B hybrid host to the first excited state. It is more specifically attributed to π-π* transition of the aromatic ring (phenSi unit). Besides, it is also observed that the broad bands are overlap with the luminescence excitation spectra (in Fig. 7) completely. It can be predicted that the energy match between organic ligand and RE^{3+} is appropriate so that phen functionalized Si-O host can absorb abundant energy in ultraviolet–visible range to transfer the energy to the corresponding hybrid materials. In addition, the introduc-

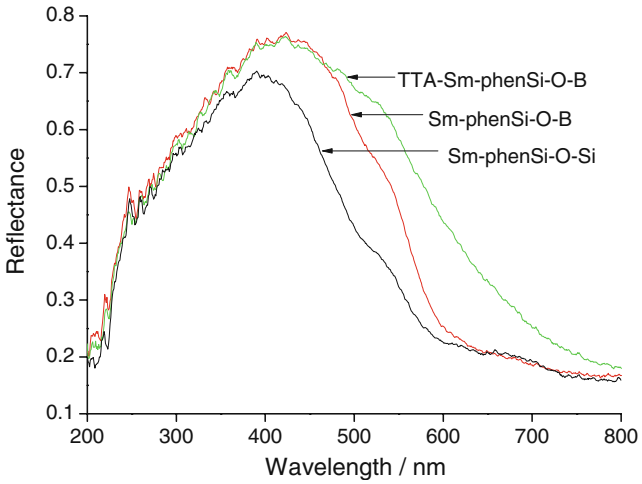

Fig. 6 The selected ultraviolet diffuse reflectance spectra of samarium hybrid gels

tion of TTA makes the side of the UV-visible absorption to move to broader range in visible region, suggesting that TTA is favorable for the energy absorption and transfer for the hybrid system.

Figure 7(a) shows the excitation and emission spectrum of europium hybrid xerogel. For excitation spectra, a broad excitation band at the range of 220 to 450 nm, suggesting the effective absorption of Eu-phen centered system. These wide excitation bands can be attributed to the organically modified Si-O-Si or Si-O-B hybrid host [38]. Here the organically modified Si-O-B or Si-O-Si hybrid hosts behave as not only host but also ligands for the coordination bonds between phenSi-O-Si(B) and Eu^{3+} [39]. The absorption of photoactive organically modified phen group and -Si-O-B(Si)- network both play role for the energy transfer and luminescence of Eu^{3+} within the hybrid gel systems. Besides, the sharp narrow lines located at long wavelength region are too weak to be observed for the transitions within $4f^6$ configurations of Eu^{3+}. The corresponding emission spectra also show the similar results in spit of that the energy transfer from phenSi to Eu(III) both occur within these two kinds of hybrid systems. As far as excitation spectra are concerned, these hybrid xerogels exhibit characteristic emissions of Eu ions. Four narrow emission peaks centered at 582, 591, 613, 651 nm, assigned to $^5D_0 \rightarrow {}^7F_0$ $^5D_0 \rightarrow {}^7F_1$, $^5D_0 \rightarrow {}^7F_2$, $^5D_0 \rightarrow {}^7F_3$ transitions, respectively. Among the peaks, the emission at 613 nm from the $^5D_0 \rightarrow {}^7F_2$ induced electronic dipole transition is the strongest, suggesting the chemical environment around Eu(III) ions has not an inversion center [40, 41]. The intensity (the integration of the luminescent band) ratio of the $^5D_0 \rightarrow {}^7F_2$ transition to $^5D_0 \rightarrow {}^7F_1$ transition has been widely used as an indicator of Eu^{3+} site symmetry [42]. When the interactions of the europium complex with its local chemical environment are stronger,

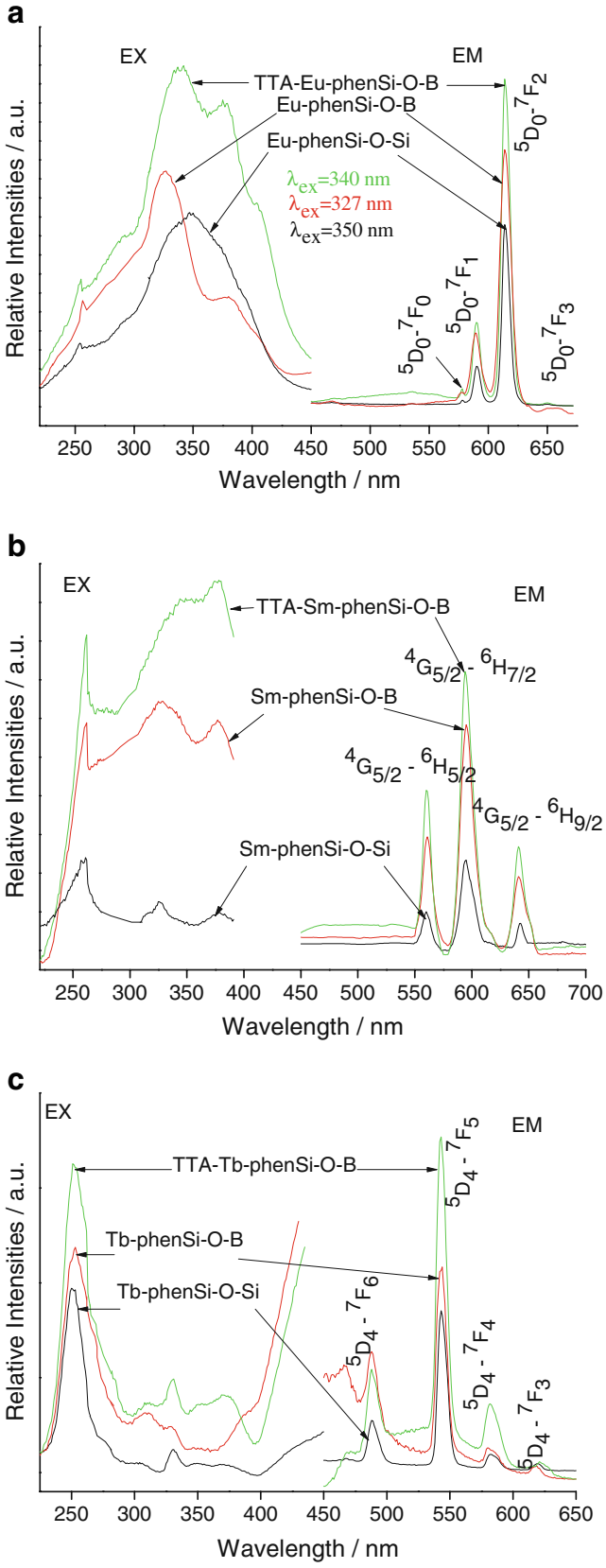

Fig. 7 The selected excitation and emission spectra of (**a**) europium, (**b**) samarium and (**c**) terbium (A) hybrid gels

the complex becomes more nonsymmetrical and the intensity of the electric-dipolar transitions becomes more intense. As a result, $^5D_0 \rightarrow {}^7F_1$ transition (magnetic-dipolar transitions) decreased and $^5D_0 \rightarrow {}^7F_2$ transition (electric-dipolar transitions) increased. The intensity ratios of $I(^5D_0 \rightarrow {}^7F_2)/I(^5D_0 \rightarrow {}^7F_1)$ (I_{02}/I_{01}, Red/Orange) for the hybrid gel Eu-phenSi-O-B is lower than that for the hybrid gel with single Si-O-Si host, and this ratio of TTA-Eu-phen-Si-O-B hybrid xerogel are slightly higher than that of Eu-phenSi (or TTA-Eu-phenSi-O-Si). But these distinctions are not both apparent, suggesting the substitution of Si by B still keep the similar chemical environment of the whole hybrid host system for that B and Si are the diagonal elements in the Periodic Table of Elements to show the similar feature and chemical behavior. This point can be verified form the sol–gel process of their alkoxy compounds [29, 43].

Figure 7(b) exhibits the excitation and emission spectra of samarium hybrid xerogels. The excitation spectra that collected at the emission wavelength of 597 nm show the similar feature to those of Eu^{3+} hybrid systems. A broad band appears in the short ultraviolet region within the range between 220 and 400 nm, which can be attributed to the organically modified phenSi framework. The excitation lines in the long wavelength region originated from the intra-configurational 4*f*–4*f* transitions of Sm^{3+} are too weak to be checked. Under the excitation, they all show the predominant characteristic emission of Sm^{3+}, which are located at 563 nm ($^4G_{5/2} \rightarrow {}^6H_{5/2}$), 601 nm ($^4G_{5/2} \rightarrow {}^6H_{7/2}$), and 645 nm ($^4G_{5/2} \rightarrow {}^6H_{9/2}$), respectively. The emission for $^4G_{5/2} \rightarrow {}^6H_{11/2}$ transition is too weak to be checked. Among the orange transition ($^4G_{5/2} \rightarrow {}^6H_{7/2}$) exhibits the strongest emission. Besides, similar to Eu hybrids, the binary hybrids of Sm-phenSi-O-B shows the slightly stronger intensity than that Sm-phenSi-O-Si, and the ternary hybrids TTA-phenSi-O-B present the stronger intensity than that of binary ones. Figure 7(c) presents the selected excitation and emission spectrum of terbium hybrid xerogels. Different from the excitation spectra of Eu and Sm hybrids, one broad excitation bands at 252 nm can be observed, corresponding to the host absorption of Si-O network, while the f-f excitation bands are too weak to be checked. Subsequently, the strong green luminescence can be observed in their emission spectra excited by 252 nm. The emission lines of the hybrid materials are assigned to the transitions from the $^5D_4 \rightarrow {}^7F_J$ (J=6, 5, 4, 3) transitions at around 489, 543, 582 and 623 nm for terbium ions. Among these emission peaks, the green luminescence ($^5D_4 \rightarrow {}^7F_5$) is most striking, which indicated that the effective energy transfer take place between phenSi and the chelated Tb ions. It is obviously different between the intensities of the green and the blue emission since the green emission is stronger than that of the blue one. The reason may be that the emission to $^5D_4 \rightarrow {}^7F_6$ is an electronic dipole transition, which is greatly influenced by the ligand field, while the emission to $^5D_4 \rightarrow {}^7F_5$ belongs to a magnetic dipole transition, which is less influenced by the ligand field. Besides, these bands in the short wavelength region cannot clearly found in the spectra of terbium hybrids, suggesting that there exist less effective energy transfer process in the terbium hybrids than europium ones.

Furhterly, the typical decay curve of the Eu^{3+} hybrid materials are measured and they can be described as a single exponential ($\mathrm{Ln}(S(t)/S_0) = -k_1 t = -t/\tau$), indicating that all Eu^{3+} ions occupy the same average coordination environment. The resulting lifetime data of Eu^{3+} hybrid materials are given in Table 1. It is found that the binary hybrid gel Eu-phenSi-O-B shows the slightly longer luminescent lifetimes than the single hybrid xerogel of Eu-phenSi-O-Si hybrid host. In addition, the luminescent lifetimes of all the ternary hybrid xerogel TTA-Eu-phenSi-O-B is longer than that of the binary hybrid gels Eu-phenSi-O- B. So the introduction of TTA is favorable for the energy transfer and luminescence of Eu^{3+} within the hybrid gels. Here the ternary hybrid gels belong to the ternary europium complexes with complicated phen organically

Table 1 The luminescent data for selected europium hybrid gel

	Eu-phenSi-O-Si	Eu-phenSi-O-B	TAA-Eu-phenSi-O-B
υ_{00} (cm^{-1})[a]	17300	17304	17304
υ_{01} (cm^{-1})[a]	16949	16978	16949
υ_{02} (cm^{-1})[a]	16287	16287	16287
$I_{02}{}^b I_{01}{}^b$	4.85	4.25	4.39
A_{00} (s^{-1})	5.40	5.62	6.09
A_{01} (s^{-1})	50.00	50.00	50.00
A_{02} (s^{-1})	252.41	221.74	228.74
τ (μs)[c]	337	356	553
A_{rad} (s^{-1})	307.81	277.36	284.83
η (%)	10.4	9.9	15.8

[a] The energies of the $^5D_0 \rightarrow {}^7F_J$ transitions (υ_{0J})

[b] The integrated intensity of the $^5D_0 \rightarrow {}^7F_J$ emission peaks

[c] The luminescence decay times of $^5D_0 \rightarrow {}^7F_2$ transitions

modified gel (ligand) and TTA (second ligand), so it is the same for that phen can also play a role to sensitize the luminescence of Eu^{3+}.

Furtherly, we determined the emission quantum efficiencies of the $^5D_0$ europium ion excited state for Eu^{3+} hybrid gel on the basis of the emission spectra and lifetimes of the $^5D_0$ emitting level using the four main equations according to the ref. [44–47]. The detailed principle and method is adopted as ref. [44] and the data are shown in Table 1.

$$A_{0J} = A_{01}(I_{0J}/I_{01})(\upsilon_{01}/\upsilon_{0J}) \quad (1)$$

$$A_{\mathrm{rad}} = \Sigma A_{0J} = A_{00} + A_{01} + A_{02} + A_{03} + A_{04} \quad (2)$$

$$\tau = {A_{\mathrm{rad}}}^{-1} + {A_{\mathrm{nrad}}}^{-1} \quad (3)$$

$$\eta = A_{\mathrm{rad}}/(A_{\mathrm{rad}} + A_{\mathrm{nrad}}) \quad (4)$$

Here A_{0J} is the experimental coefficients of spontaneous emissions (J=0, 1, 2, 3, 4)) for the branching ratio for the $^5D_0 \rightarrow {}^7F_{5,\ 6}$ transitions can be neglected as they both are not detected experimentally, whose influence can be ignored in the depopulation of the $^5D_0$ excited state [44-47]. Among A_{01} is the Einstein's coefficient of spontaneous emission between the $^5D_0$ and $^7F_1$ energy levels. In vacuum, A_{01} as a value of 14.65 s^{-1}, when an average index of refraction n equal to 1.506 is considered, the value of A_{01} can be determined to be 50 s^{-1} approximately ($A_{01} = n^3 A_{01\ (\mathrm{vacuum})}$) [44] and as a reference to calculate the value of other A_{0J}. I is the emission intensity and can be taken as the integrated intensity of the $^5D_0 \rightarrow {}^7F_J$ emission bands. υ_{0J} refers to the energy barycenter of each transition 0-J (J=0, 1, 2, 3, 4) and can be determined from the emission bands of Eu^{3+}'s $^5D_0 \rightarrow {}^7F_J$ emission transitions. A_{rad} and A_{nrad} mean to the radiative transition rate and nonradiative transition rate, respectively, among A_{rad} can be determined from the summation of A_{0J} (Eq. 2). And then the luminescence quantum efficiency can be calculated from the luminescent lifetimes, radiative and nonradiative transition rates. From the data of Table 1, it is found that the hybrid gel both of Si-O-B hybrid host (9.9%) and single Si-O-Si host (10.4%) exhibit the similar luminescent quantum efficiencies, suggesting that both Si-O-B and Si-O-Si host are benefit for the luminescence of Eu^{3+} ions. In addition, the luminescent quantum efficiencies of the ternary hybrid gel TTA-Eu-phenSi-O-B (15.8%) is higher than those of the binary hybrid gel Eu-phen-Si-O-B, revealing the introduction of TTA are favorable for the luminescence of Eu^{3+} within the hybrid systems.

Conclusions

In summary, binary and ternary rare earth (Sm^{3+}, Eu^{3+}, Tb^{3+}) hybrid xerogel with composite Si-O-B host have been prepared and compared to study with that of single host Si-O-Si through the functionalized phen linkage. The physical characterization, especially the photoluminescent properties of these hybrid gels are discussed in detail. It is found that the hybrid xerogel with composite Si-O-B host possess the superior luminescent behaviors (luminescent intensity, lifetimes and quantum efficiency) for the similar chemical nature of B to Si.

Acknowledgements This work is supported by the National Natural Science Foundation of China (20971100) and Program for New Century Excellent Talents in University (NCET 2008-08-0398).

References

1. Silver J, Withnall R (2004) Probes of structural and electronic environments of phosphor activators: Mossbauer and Raman spectroscopy. Chem Rev 104:2833
2. Kido J, Okamoto Y (2002) Organo lanthanide metal complexes for electroluminescent materials. Chem Rev 102:2357
3. Chen ZG, Chen HL, Hu H, Yu MX, Li FY, Zhang Q, Zhou ZG, Yi T, Huang CH (2008) Versatile synthesis strategy for carboxylic acid-functionalized upconverting nanophosphors as biological labels. J Am Chem Soc 130:3023
4. Ropp RC (2004) Luminescence and the solid state. Elsevier Science, 2 edn
5. Kitai A (2008) Luminescent materials and applications. Wiley
6. Eliseeva ESV, Bunzli JCG (2010) Lanthanide luminescence for functional materials and bio-sciences. Chem Soc Rev 39:189
7. Wilkinson AJ, Maffeo D, Beeby A, Foster CE, Williams JAG (2007) Sensitization of Europium(III) luminescence by benzophenone-containing ligands: regioisomers, rearrangements and chelate ring size, and their influence on quantum yields. Inorg Chem 46:9438
8. Matthews LR, Knobbe ET (1993) Luminescence behavior of europium complexes in sol-gel derived host materials. Chem Mater 5:1697
9. Klonkowski AM, Lis S, Pietraszkiewicz M, Hnatejko Z, Czarnobaj K, Elbanowski M (2003) Luminescence properties of materials with Eu(III) complexes: role of ligand, coligand, anion, and matrix. Chem Mater 15:656
10. Sanchez C, Ribot F (1994) Design of hybrid organic-inorganic materials synthesized via sol-gel chemistry. New J Chem 18:1007
11. Lenaerts PP, Storms A, Mullens J, D'Haen J, Gorller-Walrand C, Binnemans K, Driesen K (2005) Thin films of highly luminescent rare earth complexes covalently linked to an organic-inorganic hybrid material via 2-substituted imidazo(4, 5-f)-1, 10-phenanthroline groups. Chem Mater 17:5194
12. Carlos LD, Ferreira RAS, Bermudez VD, Ribeiro JLS (2009) Lanthanide-containing light-emitting organic–inorganic hybrids: a bet on the future. Adv Mater 21:509
13. Binnemans K (2009) Lanthanide-based luminescent hybrid materials. Chem Rev 109:4283
14. Franville AC, Zambon D, Mahiou R, Troin Y (2000) Luminescence behavior of sol-gel-derived hybrid materials resulting from covalent grafting of a chromophore unit to different organically modified alkoxysilanes. Chem Mater 12:428

15. Li HR, Lin J, Zhang HJ, Fu LS, Meng QG, Wang SB (2002) Preparation and luminescence properties of hybrid materials containing europium(III) complexes covalently bonded to a silica matrix. Chem Mater 14:3651
16. Carlos LD, Ferreira RAS, Pereira RN, Assuncao M, Bermudez VD (2004) White-light emission of amine-functionalized organic/inorganic hybrids: emitting centers and recombination mechanisms. J Phys Chem B 108:14924
17. Wang QM, Yan B (2004) Novel luminescent terbium molecular-based hybrids with modified meta aminobenzoic acid covalently bonded with silica. J Mater Chem 14:2450
18. Wang QM, Yan B (2005) A novel way to luminescent terbium molecular-scale hybrid materials: modified heterocyclic ligands covalently bonded with silica. Cryst Growth Des 5:497
19. Liu JL, Yan B (2008) Lanthanide (Eu^{3+}, Tb^{3+}) centered hybrid materials using modified functional bridge chemical bonded with silica: molecular design, physical characterization and photophysical properties. J Phys Chem B 112:10898
20. Yan B, Lu HF (2008) Lanthanide centered covalently bonded hybrids through sulfide linkage: molecular assembly, physical characterization and photoluminescence. Inorg Chem 47:5601
21. Yan B, Wang QM (2008) First two luminescent molecular hybrids composed of bridged Eu(III) β−diketone chelates covalently trapped in silica and titanate gels. Cryst Growth Des 6:1484
22. Lu HF, Yan B, Liu JL (2009) Functionalization of calix[4]arene as molecular bridge to assemble novel luminescent lanthanide supramolecular hybrid systems. Inorg Chem 48:3966
23. Guo L, Yan B (2010) Chemical-bonding assembly, physical characterization, and photophysical properties of rare earth hybrids from a functional thiazole bridge. Eur J Inorg Chem 1267
24. Sun LN, Zhang HJ, Peng CY, Yu JB, Meng QG, Fu LS, Liu FY, Guo XM (2006) Covalent linking of near-infrared luminescent ternary lanthanide (Er^{3+}, Nd^{3+}, Yb^{3+}) complexes on functionalized mesoporous MCM-41 and SBA-15. J Phys Chem B 110:7249
25. Li Y, Yan B, Yang H (2008) Construction, characterization and photoluminescence of mesoporous hybrids containing europium (Ш) complexes covalently bonded to SBA-15 directly functionalized by modified β-diketone. J Phys Chem C 112:3959
26. Yan B, Qiao XF (2007) Rare earth/inorganic/organic polymeric hybrid materials: molecular assembly, regular microstructure and photoluminescence. J Phys Chem B 111:12362
27. Qiao XF, Zhang HY, Yan B (2010) Photoactive binary and ternary lanthanide (Eu^{3+}, Tb^{3+}, Nd^{3+}) hybrids with p-tert-butylcalix[4] arene derived Si-O linkages and polymers. Dalton Trans 39:8882
28. Liu P, Li HR, Wang YG, Liu BY, Zhang WJ, Wang YJ, Yan WD, Zhang HJ, Schubert U (2008) Europium complexes immobilization on titania via chemical modification of titanium alkoxide. J Mater Chem 18:735
29. Yan B, Wang C, Guo L, Liu JL (2010) Photophysical properties of Eu(III) center covalently immobilized in Si-O-B and Si-O-Ti hybrid gels. Photochem Photobiol 86:499
30. Lecomte JP, Mesmaeker AKD, Demeunynck M, Lhomme J (1993) Synthesis and characterization of a new DNS-binding bifunctional ruthenium(II) complex. J Chem Soc Faraday Trans 89:3261
31. Nakamoto K (2009) Infrared and Raman spectra of inorganic and coordination compounds, part a theory and applications in inorganic chemistry, 6th Edn. Wiley-Interscience
32. Guan KS, Yin YS (2005) Effect of rare earth addition on super-hydrophilic property of $TiO2/SiO_2$ hybrid film. Mater Chem Phys 92:10
33. Yan B, Wang FF (2007) Molecular design and photo-physics of quaternary hybrid terbium centered systems with novel functional di-urea linkages of strong chemical bonds through hydrogen transfer addition. J Organomet Chem 692:2395
34. Kim JH, Lee YM (2001) Gas permeation properties of poly (amide-6-b-ethyleneoxide)-silica hybrid membranes. J Membr Sci 193:209
35. Hoffmann HS, Staudt PB, Costa TMH, Moro CC, Benvenutti EV (2002) FTIR study of the electronic metal-support interactions on platinum dispersed on silica modified with titania. Surf Interface Anal 33:631
36. Kim WS, Kim MG, Ahn JH, Bae BS, Park CB (2007) Protein micropatterning on bifunctional organic−inorganic sol−gel hybrid materials. Langmuir 23:4732
37. Ferreira RAS, Carlos LD, Goncaülves RR, Ribeiro SJL, Bermudez VD (2001) Energy-transfer mechanisms and emission quantum yields in Eu^{3+}-based siloxane-poly(oxyethylene) nanohybrids. Chem Mater 13:2991
38. Regulacio MD, Pablico MH, Vasquez JA, Myers PN, Gentry S, Prushan M, Tam-Chang SW, Stoll SL (2008) Luminescence of Ln (III) dithiocarbamate complexes (Ln) La, Pr, Sm, Eu, Gd, Tb, Dy). Inorg Chem 47:1512
39. Kawa M, Frechet JMJ (1998) Self-assembled lanthanide-cored dendrimer complexes: enhancement of the luminescence properties of lanthanide ions through site-isolation and antenna effects. Chem Mater 10:286
40. Lenaerts P, Driesen K, Van Deun R, Binnemans K (2005) Covalent coupling of luminescent tris(2-thenoyltrifluoroacetonato) lanthanide(III) complexes on a merrifield resin. Chem Mater 17:2148
41. Binnemans K, Van Herck K, Gorller-Walrand C (1997) Influence of dipicolinate ligands on the spectroscopic properties of europium(III) in solution. Chem Phys Lett 266:297
42. Wang Z, Wang J, Zhang HJ (2004) Luminescent sol-gel thin films based on europium-substituted heteropolytungstates. Mater Chem Phys 87:44
43. Nogami M, Moriya Y (1982) Glass-Formation of the SiO_2-B_2O_3 system by the gel process from metal alkoxides. J Noncryst Solids 48:359
44. Soares-Santos PCR, Nogueira HIS, Felix V, Drew MGB, Ferreira RAS, Carlos LD, Trindade T (2003) Novel lanthanide luminescent materials based on complexes of 3-hydroxypicolinic acid and silica nanoparticles. Chem Mater 15:100
45. Teotonio EES, Espinola JGP, Brito HF, Malta OL, Oliveria SF, de Foria DLA, Izumi CMS (2002) Influence of the N-[methylpyridyl] acetamide ligands on the photoluminescent properties of Eu(III)-perchlorate complexes. Polyhedron 21:1837
46. Werts MHV, Jukes RTF, Verhoeven JW (2002) The emission spectrum and the radiative lifetime of Eu^{3+} in luminescent lanthanide complexes. Phys Chem Chem Phys 4:1542
47. Lima PP, Nobre SS, Freire RO, Junior SA, Mafra L, Ferreira RAS, Pischel U, Malta OL, Carlos LD (2007) Energy transfer mechanisms in organic-inorganic hybrids incorporating europium (III): a quantitative assessment by light emission spectroscopy. J Phys Chem C 111:17627